Promote Dual-Targeting Anticancer Effect by Regulating the Dynamic Intracellular Self-Assembly

Shijin Zhang, and Ye Zhang*

Bioinspired Soft Matter Unit, Okinawa Institute of Science and Technology Graduate University, 1919-1 Tancha, Onna Son, Okinawa 904-0495, Japan.

ABSTRACT Despite the promise of nanomedicine in the fight against complex diseases, the enthusiasm for its pharmaceutical development is backed by the elevated costs associated with the R&D process. Therefore, as a compromise solution, nanotechnology was mainly applied as drug delivery system to improve bioavailability and controllability of pharmaceutical drugs. Attempting to break the restrictions without elevating potential costs, we multiply the functions of excipients in nanodelivery system by endowing subcellular-targeting ability. To prove the concept, fluorescent endoplasmic reticulum-targeted short peptides were covalently connected to chemotherapy medication Chlorambucil achieving enhanced drug loading efficiency. Via visualized intracellular dynamic enzyme-catalyzed hydrolysis, ER-targeting excipient and nucleus-targeting Chlorambucil are released simultaneously, reaching synergistic anticancer effect and elucidating the influence of intracellular self-assembly transition on enzymatic reactions.

INTRODUCTION

Nanotechnology-based drug development has made important contributions in cancer treatment during the past decades,[1-3] while most drug research still concentrated on small molecules since they have long been associated with biological discoveries.[4] Over 50% of the FDA-approved cancer drugs are protein targeted small molecules,[5] even though the poor bioavailability and the target-based resistance limit their applications. To improve the biocompatibility of small molecules, a nanoscale drug delivery system called small-molecule nanomedicine[6] assembled by small pharmaceutical molecules with minimum non-toxic excipients is constructed to enhance drug loading efficiency. Applying drug combinations to target multiple components of biological regulatory circuits produces stronger treatment, combating drug resistance.[7] Meanwhile, molecular self-assembly in cell milieu is emerging as another practical strategy for multi-component targeting nanomedicine without developing drug resistance,[8-11] although the dynamics of self-assembly in vitro is still obscure.[12-13] Enzyme-instructed assembly developed by Xu and co-workers has been widely utilized in the regulation of cell behavior with antitumor activities.[14] This strategy creates modulated and dynamic alteration of functions of assembled objects from rather simple molecular sources facilitating nanomedicine development.[15] Unfortunately, further investment beyond traditional R&D for drug development hinders the progress of such nanomedicine. Based on the statement of James Black that "the best way to discover a new drug is to start with an old one",[16] we developed a strategy of producing advanced version of small-molecule nanomedicine for multi-targeting (endoplasmic reticulum (ER) and nucleus) combination therapy (Scheme 1).[17]
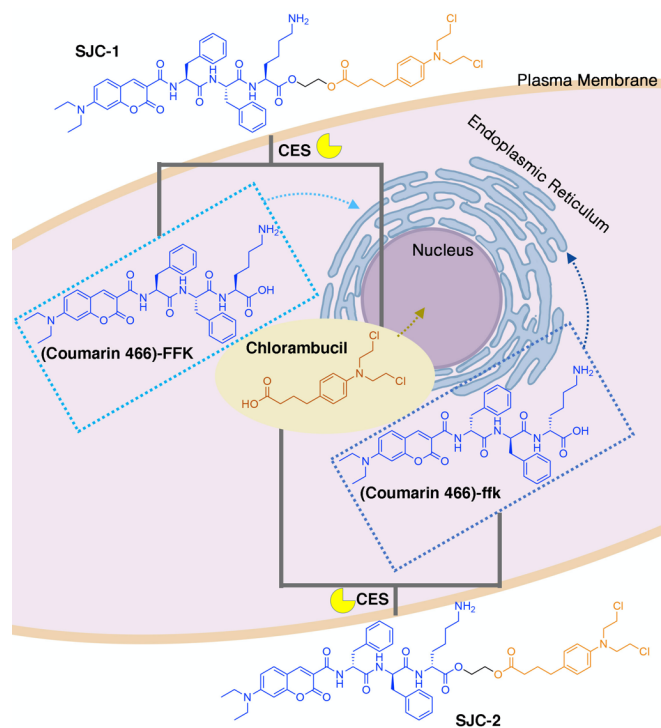
Scheme 1. Schematic illustration of self-assembling molecule design for ER and nucleus dual-targeting cancer treatment.

EXPERIMENTAL SECTION

CES-catalyzed hydrolysis of synthetic molecules in buffer. Carboxylesterase (CES) as lyophilized powder was purchased from Sigma-Aldrich (E0887). Following the enzymatic assay of esterase, CES stock solution (0.2 U/ μL) in borate buffer (pH 8.0) was prepared. 100 μM solution of **SJC-1** or **SJC-2** was prepared by diluting its DMSO solution (40 mM) with borate buffer. The CES stock solution was added into a solution of molecule to reach a final concentration of 5 U/mL. And the mixture solution was kept at 37 °C. High performance liquid chromatography (HPLC) and Mass spectrometry (MS) were applied to record the kinetic progress of hydrolysis reactions.

CES catalyzed hydrolysis of synthetic molecules in vitro. MCF-7 cells were cultured in 35 mm polystyrene culture dish. When cells reached approximately 80% confluence in the log phase growth period, culture media were aspirated and the cells were gently washed using 1x PBS buffer. After removing the washing buffer, 2 mL culture medium containing **SJC1** or **SJC2** at a concentration of 30 µM, (Coumarin 466)-FFK-Ace and (Coumarin 466)-ffk-Ace were added into the culture dish. Treated MCF-7 cells were incubated at 37°C with a humidified atmosphere of 5% CO_2 for 6 hours. Media were aspirated and the gently washed by cooling down 1x PBS buffer for 3 times. 1 mL mixture of cold MeOH and 1x PBS solution (1:1) was added into the wells and scratched to harvest the MCF-7 cells. The obtaining cell suspensions were sonicated for 10 min, 20s pulse after every 10s interval at 0 °C to break the cell membrane, centrifuged at 20000 rpm for 5 min at 4 °C, and then collected the supernatant. The supernatants were analysed using HPLC-MS to study the intracellular CES catalysed hydrolysis.

UV-Vis absorption and fluorescence emission spectroscopy. UV-Vis absorption measurement was carried out using a NanoDrop 2000C spectrophotometer (Thermo Scientific). The cuvette has a 0.5 cm path length. The detection range was set to 250-700 nm with a spectral resolution of 1.0 nm. Emission spectra were collected using a custom-made fluorescence spectrophotometer (Hamamatsu Photonics). The excitation wavelength was set to 405 nm and emission collection range was set between 415 and 750 nm.

Transmission electron microscopy (TEM). TEM imaging was carried out using a JEM-1230R (JEOL, Japan) electron microscope. Specimen was prepared following procedure: carbon-coated copper grids were glow discharged to enhance hydrophilicity; 5 µL sample solution was placed on the grid for about 60s and the excess fluid was removed using filter paper; the grid was washed using 5 µL distilled water for 3 times and the excess water was removed by a filter

paper; 5 µL uranyl acetate (1%) was placed on the grid for 20s and the excess staining solution was removed by touching the edge of grid using a filter paper; the grid was washed using 5 µL distilled water; the grid was dried at room temperature before it is ready for imaging.

Circular dichroism (CD) spectroscopy. CD spectra were recorded using a CD spectrophotometer (JASCO J-820) with bandwidth of 1.0 nm in the region (200-550 nm) under the nitrogen atmosphere. The cuvette has a 1 mm path length.

Cell culture. HeLa, SKOV3, OVCAR-3, MCF-7 cell lines were purchased from American Type Culture Collection (ATCC, USA) and cultured in ATCC recommended media. Histone H2B-GFP expressing HeLa cell line (SCC117) was purchased from Merck Millipore. HeLa cell lines were cultured in DMEM containing 10% FBS; SKOV3 cells were cultured in McCoy's medium with 10% FBS; OVCAR-3 cells were cultured in RPMI 1640 medium with 20% FBS and MCF-7 cells were cultured in EMEM with 0.01 mg/mL insulin and 10% FBS. Cell incubation was carried out at 37 °C with a humidified atmosphere of 5% CO_2. The cells were maintained at 80% confluency and used for the bioassays.

Confocal imaging. HeLa or MCF-7 cells (1×10^5) were seeded in 35mm glass bottom dish. The cells were allowed to attach for 24 h at 37 °C under 5% CO_2. The culture media were removed and changed to fresh media containing (Coumarin 466)-FFK, (Coumarin 466)-ffk, **SJC-1**, **SJC-2**, (Coumarin 466)-FFK-Ace or (Coumarin 466)-ffk-Ace at a concentration of 20 µM. After incubation for 2 h, cells were washed using 1× PBS buffer three times and stained with commercial fluorescent dyes including ER-Tracker™ Red (BODIPY™ TR Glibenclamide) and Lyso-Tracker™ Red DND-99 from ThermoFisher. After removing the staining solution, the cells were washed three times using 1× PBS buffer. The cells were observed in Cell Imaging Solution using a Nikon A1 confocal microscope.

Flow cytometry analysis of cell cycle distribution. HeLa cells (1×10^5) were seeded in 6-well plates and allowed to attach for 24 hours at 37 ºC under 5% CO_2. The cells were treated with **SJC-1** or **SJC-2** at a concentration of 20 µM for various durations (6 h, 12 h, and 24 h). Untreated HeLa cells were used as control. Cells were harvested by trypsin and washed twice using ice-cold 1× PBS buffer. The cells were further fixed with 70% ethanol at 4 ºC overnight and treated with RNase A for 30 min at 37 ºC, followed by PI staining for 30 min in the dark at room temperature. Cell cycle analysis was carried out using flow cytometer (Merck Millipore ImageStream X Mark II), and 2×10^4 events per sample were counted.

Cell viability assay. For all cell lines, 1×10^4 cells per well in exponential growth phase were seeded in a 96 well plate. The cells were allowed to attach to the wells at 37 ºC, 5% CO_2 for several hours. The culture media were removed followed by addition of 100 µL culture media containing compound (Coumarin 466)-FFK, (Coumarin 466)-ffk, **SJC-1**, **SJC-2**, (Coumarin 466)-FFK-Ace, (Coumarin 466)-ffk-Ace, chlorambucil (immediately diluted from 80 mM stock solution in DMSO), the mixture of chlorambucil/(Coumarin 466)-FFK (1:1) or chlorambucil/(Coumarin 466)-ffk (1:1), and Cisplatin at different concentrations. After incubation, 10 µL MTT solution (5 mg/mL) was added to each well and incubated at 37 °C for 4 h. Then 100 µL SDS solution (10% in Milli-Q water) was added to each well to stop the reduction reaction and dissolve the purple formazan. The absorbance at 570 nm was measured using Nivo3 microplate reader (PerkinElmer). All experiments were performed in triplicate and repeated three times.

Western blotting. 5.0×10^5 MCF-7 cells per well were seeded in 6-well plate and allowed to attach for 24 hours. The cells were treated with 0, 5, 10 and 20 µM **SJC-1** and **SJC-2**; 0, 10, 25 and 50 µM (Coumarin 466)-FFK-Ace and (Coumarin 466)-ffk-Ace for 12 hours. The cells were

harvested and washed using 1× ice cold PBS twice. 70μL CelLytic M solution (Sigma-Aldrich) containing protease inhibitors cocktail was added to the cells for 30 min incubation on a shaker at 0 °C. Then centrifuge the lysed cells for 5 min at 20000 rmp (4 °C) to pellet the cellular debris. The protein concentrations of lysates were determined via the bicinchoninic acid (BCA) method. Proteins were dissolved in SDS sample buffer containing 2% β-mercaptoehtanol. Samples (10 μg of protein, ~ 10 μL) were loaded and separated by 10% Laemmli-SDS-PAGE. For Western blot analysis, the proteins were transferred onto a polyvinylidene difluoride (PVDF; Bio-Rad, Hercules, CA, USA) membrane. After blocking with Blocking one-P (Nacalai Tesque, Kyoto, Japan), the membrane was incubated with the antibody. Specifically, incubating with 1:1000 dilution for Bip, Calnexin, IRE1a and PDI (Cell Signaling Technology, #9956), and 1:2000 dilution for beta-actin (Abcam, ab8227) antibody for overnight at 4 °C. After washing, the membrane was incubated with 1000-fold diluted peroxidase-conjugated goat anti-rabbit IgG (Bio-Rad, Hercules, CA, USA) for 90 min, and then stained using ECLTM prime Western blotting detection reagent (GE Healthcare, Little Chalfont, UK).

RESULTS AND DISCUSSION

Design self-assembling molecules for dual-targeting anticancer strategy. As demonstrated in scheme 1, Chlorambucil, the small molecule chemotherapy medication with poor biocompatibility that alkylates and crosslinks DNA,[18] was selected as the 'old drug' to couple with ER-targeting, π-π stacking and hydrogen bonding oriented self-assembling molecule[17] (Coumarin 466)-FFK covalently via diester bond.[19] The obtained 'new drug' **SJC-1** is a nanoscale delivery system for high Chlorambucil loading. Upon the hydrolysis by carboxylesterase (CES) that is commonly expressed in tumor tissue,[20] Chlorambucil is released to damage DNA, and (Coumarin 466)-FFK is released to self-assemble on ER inducing ER stress.

The combination of small pharmaceutical molecule and subcellular-targeted self-assembly achieves a synergistic therapeutic effect against cancer without developing target-based resistance.[21] To explore the intracellular self-assembly dynamics and the impact on cellular response, a D-version[22-24] ER-targeting 'excipient' (Coumarin 466)-ffk is applied to couple with Chlorambucil obtaining **SJC-2** for comparison.

In water, **SJC-1** and **SJC-2** both self-assemble into clusters of irregular nanovesicles with diameters around 100 nm (Figure 1A) linked by fibrillar structures (Figure S1) at the concentration beyond 20 μM (Figure S2). The circular dichroism (CD) spectra of both molecules are specular images (Figure 1B) indicating that the chirality of the short peptide building blocks FFK/ffk is transferred supramolecularly to **SJC-1** and **SJC-2** assembled nanostructures.[25] Although they share the same chemical structures, the chirality difference leads to different kinetic profiles of CES-catalyzed hydrolysis. As indicated in Figure 1C, under the same reaction condition, **SJC-1** is hydrolyzed at a slower speed than **SJC-2**. For example, the time required for complete hydrolysis reaction of **SJC-1** is twice the time required for completed hydrolysis of **SJC-2** (Figure S3). The difference in hydrolysis dynamics is maintained inside the cell (Figure S4). Both hydrolysis reactions lead to self-assembling morphology transition from vesicle-like to film-like nanostructures (Figure 1D). The steady state absorption and emission spectra of **SJC-1** (Figure 1E) and **SJC-2** (Figure 1F) both exhibit absorption peak at 421 nm in water, whereas their hydrolyzed analogue molecules exhibit absorption peak at 433 nm. The fluorescence emission peaks of **SJC-1** and **SJC-2** were both observed at 557 nm in water. After CES-catalyzed hydrolysis, both obtained analogue molecules exhibit emission peak at 480 nm. The observed blue shift is highly possibly due to the H-type aggregation of Coumarin 466 in hydrolyzed analogues.[26] Such drastic fluorescence shift (91 nm) provides researchers the

possibility of *in situ* observation of the dynamics of intracellular self-assembly triggered by CES-catalyzed hydrolysis (Figure S5).
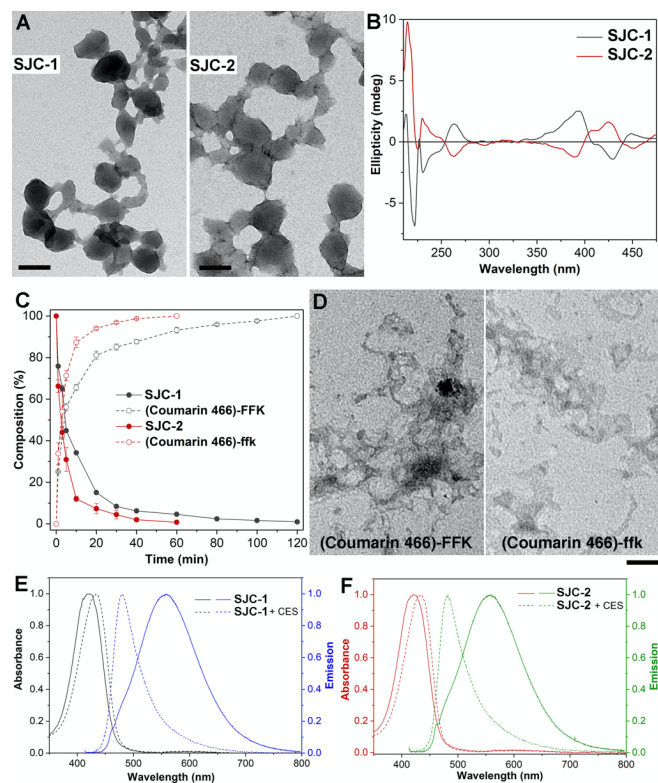
Figure 1. (A) TEM images of self-assembly of **SJC-1** or **SJC-2** in water at a concentration of 50 μM. Scale bars represent 100 nm. (B) CD spectra of **SJC-1** or **SJC-2** in water at a concentration of 200 μM. (C) Kinetic profiles of CES-catalyzed hydrolysis (5 U/mL) of **SJC-1** or **SJC-2** at a concentration of 100 μM in borate buffer (pH = 8.0) at 37 °C. (D) TEM images of self-assembly of (Coumarin 466)-FFK or (Coumarin 466)-ffk in water at a concentration of 50 μM. Normalized absorption and emission spectra of **SJC-1** (E) or **SJC-2** (F) before and after the hydrolysis by CES.

CES-triggered dual-targeting anticancer approach against multiple cancer cell lines. Upon the treatment of **SJC-1** or **SJC-2** at relative low concentration (50 μM), DNA condensation was observed after short but different period of incubation (Figure 2A and Figure

S6). **SJC-2** exhibited DNA condensation effect on HeLa cells few hours faster than SJC-1 indicating a better synergistic effect of cell uptake and chlorambucil release. The flow cytometry analysis for cell cycle distribution confirmed the mitotic arrest induced by the treatment of **SJC-1** or **SJC-2** (Figure S7). The results suggest that efficient delivery of Chlorambucil is achieved by these two small molecule nanomedicines. Confocal microscopy images of HeLa cells upon the treatment of two molecules at relatively low concentrations with reduced cell toxicity confirmed that the hydrolyzed analogue molecules (Coumarin 466)-FFK and (Coumarin 466)-ffk both accumulated on ER (Figure 2B and 2C). And the strong fluorescence signal confirmed to have high drug loading efficiency too. Via cell viability tests, the dual-targeting small-molecule nanomedicines are confirmed with high toxicity against different types of cancer cells including HeLa cells (cervical cancer) (Figure 2D), SKOV3 cells (ovarian cancer) (Figure 2E), OVCAR-3 cells (drug-resistant ovarian cancer) (Figure 2F), and MCF-7 cells (breast cancer) (Figure 2G). Even though MCF-7 cells are known for consistent resistance to alkylating agents by exhibiting close to 100% cell viability upon the treatment of Chlorambucil, (Coumarin 466)-FFK, (Coumarin 466)-ffk, and their combinations (Figure 2H),[27] **SJC-1** and **SJC-2** exhibited IC50 of 21.7 μM and 10.9 μM, respectively, much lower than the IC50 of prolidase-activated prodrug of Chlorambucil and the chemotherapy drug Cisplatin (Figure S8).[28] On all cancer cell lines, **SJC-2** exhibits higher toxicity than **SJC-1**.
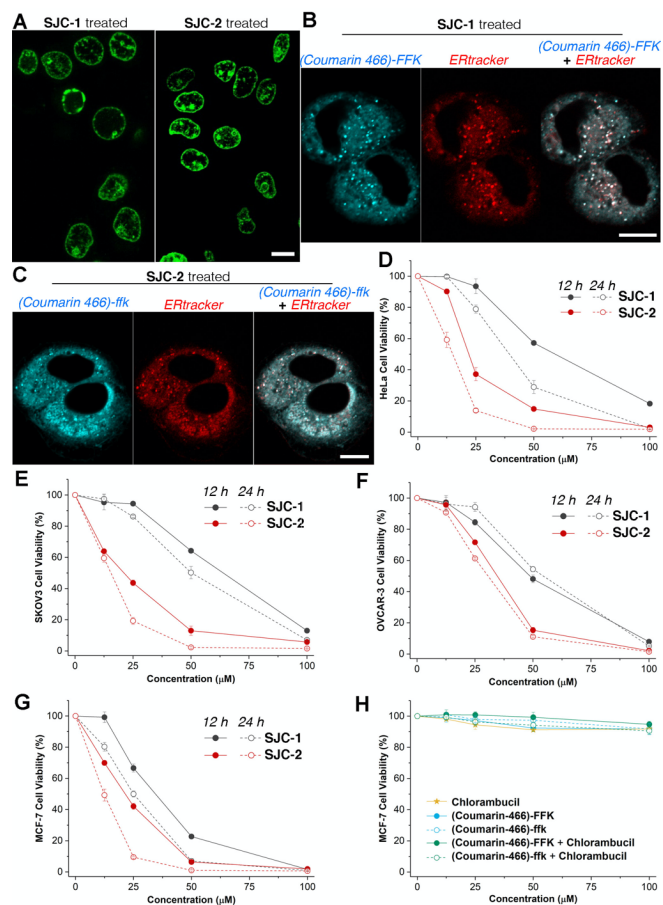
Figure 2. (A) Fluorescent images of chromatin in histone H2B-GFP expressing HeLa cells treated by **SJC-1** or **SJC-2** at a concentration of 50 μM for 4 hours. Scale bar represents 10 μm. (B) Intracellular localization of (Coumarin 466)-FFK in HeLa cells treated by **SJC-1** (20 μM) for 2 hours and co-stained with ER-tracker (red). Scale bar represents 10 μm. (C) Intracellular localization of (Coumarin 466)-ffk in HeLa cells treated by **SJC-2** (20 μM) for 2 hours and co-stained with ER-tracker (red). Scale bar represents 10 μm. 12-hour and 24-hour HeLa cell (D), SKOV3 cell (E), OVCAR-3 cell (F), and MCF-7 cell (G) viabilities upon the incubation with **SJC-1** or **SJC-2** at various concentrations. (H) 24-hour MCF-7 cell viability upon the incubation of Chlorambucil, (Coumarin 466)-FFK, (Coumarin 466)-ffk, and their mixtures at various concentrations.

11

CES-triggered molecular self-assembly induces ER-stress. Since direct treatment of (Coumarin 466)-ffk in MCF-7 cell culture failed in accumulation on ER (Figure S9), to properly examine the influence induced by ER-targeted self-assembly, two small-molecule medicines (Coumarin 466)-FFK-Ace and (Coumarin 466)-ffk-Ace as CES-instructed nanoscale delivery systems are designed and synthesized (Figure 3A). Following their static absorptions at 436 nm and fluorescent emissions around 470 nm (Figure 3B), the confocal microscopy imaging was conducted to examine intracellular localizations. Upon the treatment of these two molecules, (Coumarin 466)-FFK and (Coumarin 466)-ffk were successfully delivered to ER at high loading rate (Figure 3C and 3D) and exhibited similar concentration dependent toxicity against MCF-7 cells (Figure 3E).

The ER transmembrane sensor protein IRE1[29], ER stress regulators including ER chaperone proteins Bip[30] and Calnexin[31], and luminal ER oxidoreductase protein disulfide isomerase-A1 (PDI)[32] exhibited upregulation at different levels in MCF-7 cells upon the treatment of **SJC-1**, **SJC-2**, (Coumarin 466)-FFK-Ace, and (Coumarin 466)-ffk-Ace at increased concentrations (Figure 3F and Figure S10), which confirmed the ER-targeted self-assembly of (Coumarin 466)-FFK and (Coumarin 466)-ffk both induce ER stress triggering cell death.
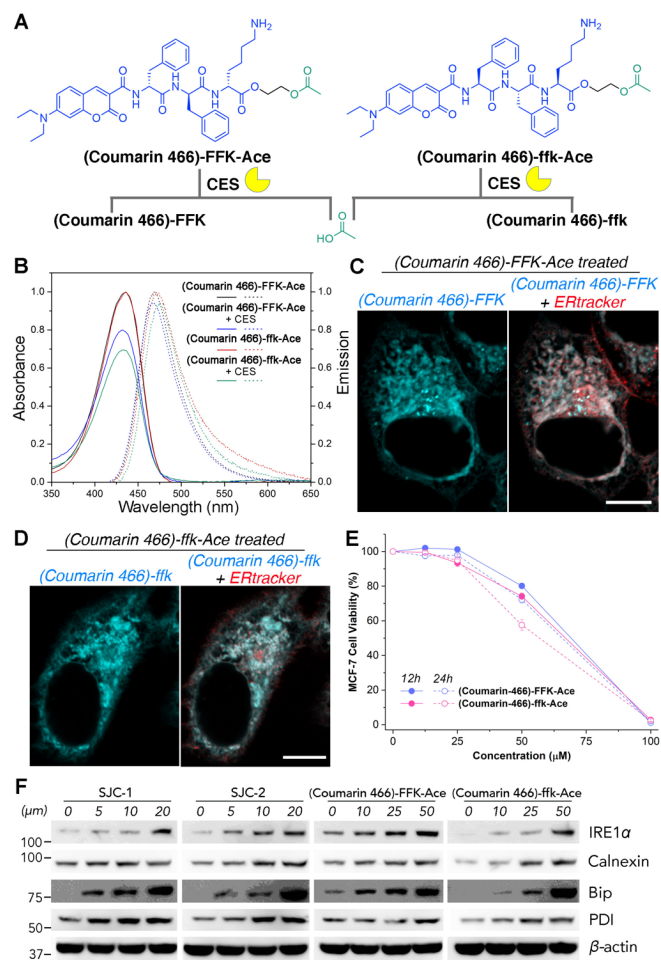
Figure 3. (A) Schematic illustration of CES-catalyzed hydrolysis of (Coumarin 466)-FFK-Ace or (Coumarin 466)-ffk-Ace. (B) Absorption and emission spectra of (Coumarin 466)-FFK-Ace or (Coumarin 466)-ffk-Ace before and after CES-catalyzed hydrolysis. (C) Intracellular localization of (Coumarin 466)-FFK in MCF-7 cells treated by (Coumarin 466)-FFK-Ace (20 μM) for 2 hours and co-stained with ERtracker (red). Scale bar represents 10 μm. (D) Intracellular localization of (Coumarin 466)-ffk in MCF-7 cells treated by (Coumarin 466)-FFK-Ace (20 μM) for 2 hours and co-stained with ERtracker (red). Scale bar represents 10 μm. (E) 12-hour and 24-hour MCF-7 cell viability upon the incubation with (Coumarin 466)-FFK-Ace or (Coumarin 466)-ffk-Ace at various concentration. (F) Immunoblotting analysis of MCF-7 cells

transiently expressing IRE1α, Calnexin, Bip, and PDI upon incubation with **SJC-1**, **SJC-2**, (Coumarin 466)-FFK-Ace, or (Coumarin 466)-ffk-Ace at various concentrations for 12 hours.

CES-triggered dynamic intracellular self-assembly. To understand the drug synergy for further optimization of beneficial drug interactions, we monitored the intracellular dynamics of CES-instructed self-assembly upon the treatment of **SJC-1** and **SJC-2** using time-lapse confocal microscopy imaging of MCF-7 cells (Figure 4A). Upon 1-hour treatment, both intracellular **SJC-1** and **SJC-2** are in reticular shape localized on ER with higher loading efficiency in **SJC-2** treatment. At the same time, CES-catalyzed hydrolysis efficiently proceeded exhibiting ER-targeted self-assembly of analogue molecules. Since 6-hour treatment, **SJC-1** gradually transformed into punctuate shape aggregates colocalized with part of the (Coumarin 466)-FFK. Zoom-in image exhibited co-existence of punctuate and reticular shape (Coumarin 466)-FFK, and the punctuates co-localized with **SJC-1** (Figure 4B). Smaller amount of punctuate aggregation of **SJC-2** was also observed after 6-hour treatment. After 12 hours, large amount of punctuate shape **SJC-1** were still remained, while most of the **SJC-2** were hydrolyzed except small amount in punctuate shape. Zoom-in image exhibited much higher accumulation rate of (Coumarin 466)-ffk on ER than (Coumarin 466)-FFK.

Regarding the intracellular morphology transition of self-assembled **SJC-1/SJC-2**, and their hydrolysis reaction rate, we tested the CES-catalyzed hydrolysis in their aggregating state in solution (Figure S11). The results indicate that the hydrolysis is severely hindered when the reactants are tightly packed. And this may well explain why the unhydrolyzed intracellular **SJC-1/SJC-2** are punctuated aggregates. Since the CES-catalyzed hydrolysis of **SJC-2** is faster than **SJC-1**, higher production rate of (Coumarin 488)-ffk than (Coumarin 488)-FFK were achieved before **SJC-2** and **SJC-1** transform into punctuate aggregates. Therefore, less unhydrolyzed

nanomedicines remained in the **SJC-2** treated MCF-7 cells, while more Chlorambucil was released for efficient DNA damaging. The higher stability of D-version peptide than the L-version also contribute to long-term higher accumulation rate of (Coumarin 488)-ffk than (Coumarin 488)-FFK raising ER stress for synergistic anticancer effect with Chlorambucil.
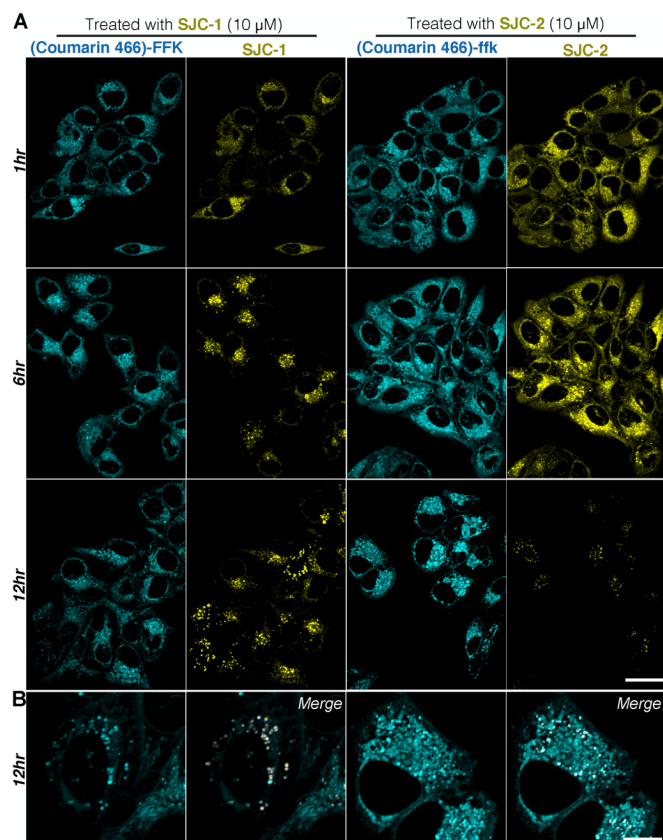
Figure 4. (A) Spatial distribution of (Coumarin 466)-FFK (ex/em: 405/420-490nm) and **SJC-1** (ex/em: 442/528-593 nm) in MCF-7 cells upon the treatment of **SJC-1** (10 μM) for 1, 6, and 12 hours. Spatial distribution of (Coumarin 466)-ffk (ex/em: 405/420-490nm) and **SJC-2** (ex/em: 442/528-593 nm) in MCF-7 cells upon the treatment of **SJC-2** (10 μM) for 1, 6 and 12 hours. Scale bar represents 30 μm. (B) Intracellular co-localization of (Coumarin 466)-FFK with **SJC-1** in MCF-7 cells upon the treatment of **SJC-1** for 12 hours, or (Coumarin 466)-ffk with **SJC-2** in MCF-7 cells upon the treatment of **SJC-2** for 12 hours.

CONCLUSIONS

The higher anticancer toxicity of D-version peptide has been very well studied.[22] And it's generally agreed that the intracellular stability is the key for the efficacy. However, the observation and comparison of dynamic self-assembly and the correlated hydrolysis rate between L-version and D-version nanomedicines in cell milieu has not been reported yet.[33] This research clearly presented the influence of self-assembly transitions on its enzyme-catalyzed hydrolysis reactions, which is essential to drug release efficiency. These correlated kinetic profiles will offer important insights into the intracellular enzyme-instructed molecular self-assembly, which will provide valuable contribution to the development of advanced nanomedicines.

ASSOCIATED CONTENT

Supporting Information. The supporting information is available free of charge on the ACS Publication website. Materials and methods, Scheme S1-S13, Figure S1-S29 (PDF).

AUTHOR INFORMATION

Corresponding Author

*Ye Zhang, Bioinspired Soft Matter Unit, Okinawa Institute of Science and Technology, Okinawa, Japan; Email: ye.zhang@oist.jp

Author Contributions

The manuscript was written through contributions of all authors. All authors have given approval to the final version of the manuscript.

Funding Sources

REFERENCES

(1)   Grodzinski, P.; Kircher, M.; Goldberg, M.; Gabizon, A., Integrating Nanotechnology into Cancer Care. *Acs Nano* **2019,** *13*, 7370-7376.

(2)   Tran, S.; DeGiovanni, P. J.; Piel, B.; Rai, P., Cancer nanomedicine: a review of recent success in drug delivery. *Clin Transl Med* **2017,** *6*, 44.

(3)   Jia, X.; Zhang, Y.; Zou, Y.; Wang, Y.; Niu, D.; He, Q.; Huang, Z.; Zhu, W.; Tian, H.; Shi, J.; Li, Y., Dual Intratumoral Redox/Enzyme-Responsive NO-Releasing Nanomedicine for the Specific, High-Efficacy, and Low-Toxic Cancer Therapy. *Adv Mater* **2018,** *30*, 1704490.

(4)   Hoelder, S.; Clarke, P. A.; Workman, P., Discovery of small molecule cancer drugs: Successes, challenges and opportunities. *Mol Oncol* **2012,** *6*, 155-176.

(5)   Santos, R.; Ursu, O.; Gaulton, A.; Bento, A. P.; Donadi, R. S.; Bologa, C. G.; Karlsson, A.; Al-Lazikani, B.; Hersey, A.; Oprea, T. I.; Overington, J. P., A comprehensive map of molecular drug targets. *Nat Rev Drug Discov* **2017,** *16*, 19-34.

(6)   Xue, X. D.; Lindstrom, A.; Qu, H. J.; Li, Y. P., Recent advances on small-molecule nanomedicines for cancer treatment. *Wires Nanomed Nanobi* **2020,** *12*.

(7)   Rationalizing combination therapies. *Nat Med* **2017,** *23*, 1113-1113.

(8)   Feng, Z. Q. Q.; Wang, H. M.; Wang, S. Y.; Zhang, Q.; Zhang, X. X.; Rodal, A. A.; Xu, B., Enzymatic Assemblies Disrupt the Membrane and Target Endoplasmic Reticulum for Selective Cancer Cell Death. *J Am Chem Soc* **2018,** *140*, 9566-9573.

(9)   Mang, D.; Zhang, S.; Wu, X.; Hu, X.; Mochizuki, T.; Li, G.; Zhang, Y., Enzyme-mediated dual-targeted-assembly realizes a synergistic anticancer effect. *Chem Commun (Camb)* **2019,** *55*, 6126-6129.

(10)   Yuan, Y.; Wang, L.; Du, W.; Ding, Z. L.; Zhang, J.; Han, T.; An, L. N.; Zhang, H. F.; Liang, G. L., Intracellular Self-Assembly of Taxol Nanoparticles for Overcoming Multidrug Resistance. *Angew Chem Int Edit* **2015,** *54*, 9700-9704.

(11)   Wang, H. M.; Feng, Z. Q. Q.; Xu, B., Bioinspired assembly of small molecules in cell milieu. *Chem Soc Rev* **2017,** *46*, 2421-2436.

(12)   Zhan, J.; Cai, Y. B.; He, S. S.; Wang, L.; Yang, Z. M., Tandem Molecular Self-Assembly in Liver Cancer Cells. *Angew Chem Int Edit* **2018,** *57*, 1813-1816.

(13)   Zheng, Z.; Chen, P. Y.; Xie, M. L.; Wu, C. F.; Luo, Y. F.; Wang, W. T.; Jiang, J.; Liang, G. L., Cell Environment-Differentiated Self-Assembly of Nanofibers. *J Am Chem Soc* **2016,** *138*, 11128-11131.

(14)   He, H.; Xu, B., Instructed-Assembly (iA): A Molecular Process for Controlling Cell Fate. *Bull Chem Soc Jpn* **2018,** *91*, 900-906.

(15)   Ariga, K.; Jia, X.; Song, J.; Hill, J. P.; Leong, D. T.; Jia, Y.; Li, J., Nanoarchitectonics beyond Self-Assembly: Challenges to Create Bio-Like Hierarchic Organization. *Angew Chem Int Ed Engl* **2020,** *59*, 2-25.

(16) Raju, T. N. K., The Nobel chronicles. *Lancet* **2000,** *356*, 81-81.

(17) Zhang, S.; Hu, X.; Mang, D.; Sasaki, T.; Zhang, Y., Self-delivery of N-hydroxylethyl peptide assemblies to the cytosol inducing endoplasmic reticulum dilation in cancer cells. *Chem Commun (Camb)* **2019,** *55*, 7474-7477.

(18) Robak, T.; Kasznicki, M., Alkylating agents and nucleoside analogues in the treatment of B cell chronic lymphocytic leukemia. *Leukemia* **2002,** *16*, 1015-1027.

(19) Fu, R. G.; Sun, Y.; Sheng, W. B.; Liao, D. F., Designing multi-targeted agents: An emerging anticancer drug discovery paradigm. *Eur J Med Chem* **2017,** *136*, 195-211.

(20) Xu, G.; Zhang, W. H.; Ma, M. K.; McLeod, H. L., Human carboxylesterase 2 is commonly expressed in tumor tissue and is correlated with activation of irinotecan. *Clin Cancer Res* **2002,** *8*, 2605-2611.

(21) Panasci, L.; Paiement, J. P.; Christodouplopoulos, G.; Belenkov, A.; Malapetsa, A.; Aloyz, R., Chlorambucil drug resistance in chronic lymphocytic leukemia: The emerging role of DNA repair. *Clin Cancer Res* **2001,** *7*, 454-461.

(22) Feng, Z.; Xu, B., Inspiration from the mirror: D-amino acid containing peptides in biomedical approaches. *Biomolecular concepts* **2016,** *7*, 179-187.

(23) Li, J.; Kuang, Y.; Gao, Y.; Du, X.; Shi, J.; Xu, B., D-amino acids boost the selectivity and confer supramolecular hydrogels of a nonsteroidal anti-inflammatory drug (NSAID). *J Am Chem Soc* **2013,** *135*, 542-545.

(24) Zhou, J.; Du, X. W.; Li, J.; Yamagata, N.; Xu, B., Taurine Boosts Cellular Uptake of Small D-Peptides for Enzyme-Instructed Intracellular Molecular Self-Assembly. *J Am Chem Soc* **2015,** *137*, 10040-10043.

(25) Yang, Y.; Zhang, Y.; Wei, Z., Supramolecular Helices: Chirality Transfer from Conjugated Molecules to Structures. *Adv Mater* **2013,** *25*, 6039-6049.

(26) Verma, P.; Pal, H., Intriguing H-Aggregate and H-Dimer Formation of Coumarin-481 Dye in Aqueous Solution As Evidenced from Photophysical Studies. *J Phys Chem A* **2012,** *116*, 4473-4484.

(27) Morrow, C. S.; Smitherman, P. K.; Diah, S. K.; Schneider, E.; Townsend, A. J., Coordinated action of glutathione S-transferases (GSTs) and multidrug resistance protein 1 (MRP1) in antineoplastic drug detoxification. Mechanism of GST A1-1- and MRP1-associated resistance to chlorambucil in MCF7 breast carcinoma cells. *J Biol Chem* **1998,** *273*, 20114-20120.

(28) Bielawska, A.; Bielawski, K.; Chrzanowski, K.; Wolczynski, S., Prolidase-activated prodrug for cancer chemotherapy cytotoxic activity of proline analogue of chlorambucil in breast cancer MCF-7 cells. *Farmaco* **2000,** *55*, 736-741.

(29) Chen, Y.; Brandizzi, F., IRE1: ER stress sensor and cell fate executor. *Trends Cell Biol* **2013,** *23*, 547-555.

(30) Lee, A. S., The ER chaperone and signaling regulator GRP78/BiP as a monitor of endoplasmic reticulum stress. *Methods* **2005,** *35*, 373-381.

(31) Guerin, R.; Arseneault, G.; Dumont, S.; Rokeach, L. A., Calnexin is involved in apoptosis induced by endoplasmic reticulum stress in the fission yeast. *Mol Biol Cell* **2008,** *19*, 4404-20.

(32) Kranz, P.; Neumann, F.; Wolf, A.; Classen, F.; Pompsch, M.; Ocklenburg, T.; Baumann, J.; Janke, K.; Baumann, M.; Goepelt, K.; Riffkin, H.; Metzen, E.; Brockmeier, U., PDI is an essential redox-sensitive activator of PERK during the unfolded protein response (UPR). *Cell Death Dis* **2017,** *8*.

(33) Gao, Y.; Shi, J. F.; Yuan, D.; Xu, B., Imaging enzyme-triggered self-assembly of small molecules inside live cells. *Nat Commun* **2012,** *3*.

TOC